ISSN 1674-1056
http://cpb.iphy.ac.cn
http://iopscience.iop.org/cpb
中国物理 B
Chinese Physics
中国物理 Chinese Physics B

Crystal structure and magnetic properties of disordered alloy $ErGa_{3-x}Mn_x$

Cong Wang(王聪), Yong-Quan Guo(郭永权), Shuo-Wang Yang(杨硕望)
Citation: Chin. Phys. B . 2019, 28(8): 086101 . **doi:** 10.1088/1674-1056/28/8/086101
Journal homepage: http://cpb.iphy.ac.cn; http://iopscience.iop.org/cpb

What follows is a list of articles you may be interested in

Isostructural phase transition-induced bulk modulus multiplication in dopant-stabilized ZrO_2 solid solution

Min Wang(王敏), Wen-Shu Shen(沈文舒), Xiao-Dong Li(李晓东), Yan-Chun Li(李延春), Guo-Zhao Zhang(张国召), Cai-Long Liu(刘才龙), Lin Zhao(赵琳), Shu-Peng Lv(吕舒鹏), Chun-Xiao Gao(高春晓), Yong-Hao Han(韩永昊)
Chin. Phys. B . 2019, 28(7): 076109 . **doi:** 10.1088/1674-1056/28/7/076109

Enhanced structural and magnetic properties of microwave sintered Li-Ni-Co ferrites prepared by sol-gel method

Nandeibam Nilima, M Maisnam, Sumitra Phanjoubam
Chin. Phys. B . 2019, 28(2): 026101 . **doi:** 10.1088/1674-1056/28/2/026101

Compression behavior and phase transition of β-Si_3N_4 under high pressure

Hong-xia Gong(龚红霞), Zi-li Kou(寇自力), Cong Fan(樊聪), Hao Liang(梁浩), Qi-ming Wang(王齐明), Lei-lei Zhang(张雷雷), Fang Peng(彭放), Ming Yang(杨鸣), Xiao-lin Ni(倪小林), Jing Liu(刘景)
Chin. Phys. B . 2018, 27(5): 056101 . **doi:** 10.1088/1674-1056/27/5/056101

Structural phase transition, strength, and texture in vanadium at high pressure under nonhydrostatic compression

Lun Xiong(熊伦), Jing Liu(刘景)
Chin. Phys. B . 2018, 27(3): 036101 . **doi:** 10.1088/1674-1056/27/3/036101

Structural, magnetic properties, and electronic structure of hexagonal FeCoSn compound

Yong Li(李勇), Xue-Fang Dai(代学芳), Guo-Dong Liu(刘国栋), Zhi-Yang Wei(魏志阳), En-Ke Liu(刘恩克), Xiao-Lei Han(韩小磊), Zhi-Wei Du(杜志伟), Xue-Kui Xi(郗学奎), Wen-Hong Wang(王文洪), Guang-Heng Wu(吴光恒)
Chin. Phys. B . 2018, 27(2): 026101 . **doi:** 10.1088/1674-1056/27/2/026101

Crystal structure and magnetic properties of disordered alloy $ErGa_{3-x}Mn_x$*

Cong Wang(王聪), Yong-Quan Guo(郭永权)†, and Shuo-Wang Yang(杨硕望)

School of Energy Power and Mechanical Engineering, North China Electric Power University, Beijing 102206, *China*

(Received 19 April 2019; revised manuscript received 17 June 2019; published online 25 July 2019)

$ErGa_{3-x}Mn_x$ disordered alloy is successfully prepared by the vacuum arc melting technology, and the crystal structure and magnetic properties are investigated by using the x-ray diffraction and magnetic measurements. The Rietveld structural analysis indicates that the $ErGa_{3-x}Mn_x$ crystallizes into a cubic structure with space group of $Pm\bar{3}m$ in Mn doping range of $x = 0$–0.1. However, the disordered alloy with structural formula of $Er_{0.8}Ga_2^I(Ga^{II}, Mn)_{0.4}$ as the second phase is separated from cubic phase for the samples with $x = 0.2$ and 0.3, which is induced by substituting the (Ga^{II}, Mn)–(Ga^{II}, Mn) pair at 2*e* crystal position for the rare earth Er at 1*a* site. The lattice parameters tend to increase with Mn content increasing due to the size effect at Ga (1.30 Å) site by substituting Mn (1.40 Å) for Ga. The paramagnetic characteristic is observed by doping Mn into $ErGa_3$ at room temperature. With Mn content increasing from $x = 0$ to 0.1, the magnetic susceptibility χ tends to increase. This phenomenon can be due to the increase of effective potential induced by doping Mn into $ErGa_3$. However, the magnetic susceptibility χ continues to decrease with the increase of Mn content in a range of $x > 0.2$, which is due to the phase separation from the cubic Er(Ga, Mn)$_3$ to the hexagonal $Er_{0.8}Ga_2$(Ga, Mn)$_{0.4}$.

Keywords: $ErGa_{3-x}Mn_x$, Rietveld structure refinement, magnetic transport

PACS: 61.05.cp, 61.50.–f, 63.50.Gh, 87.80.Lg **DOI:** 10.1088/1674-1056/28/8/086101

1. Introduction

Most of RX_3 intermetallic compounds (R = rare earth; X = In, Ga, Tl, Sn, and Pb) have a cubic $AuCu_3$-type crystal structure.[1–8] The interest in RX_3 is growing due to their salient features such as formation of magnetic moment, crystal field effect, and multiaxial magnetic structures.[9–11] In the last decade, the research activities have focused on the binary intermetallic compounds RIn_3 with cubic $AuCu_3$-type structure due to their excellent physical properties such as low temperature superconductor, complex magnetic ordering, Kondo effect, and multi-axis magnetic structure.[12–14] Gallium belongs to the IIIA group, but the RGa_3 intermetallics cannot be formed between the light rare earth and Ga. In the heavy rare earth case, the stoichiometry *R*Ga 1:3-type intermetallics only exist in a few of rare earths such as: Tm, Lu, Dy, Ho, and Er,[15,16] where $TmGa_3$, $LuGa_3$, and $ErGa_3$ crystallize into a cubic $AuCu_3$-type structure.[17] $TmGa_3$ shows a modulated antiferromagnetic structure at low temperature, it orders antiferromagnetically around 4.2 K.[18] The saturation moment of $TmGa_3$ is 6.1 μ_B at 2 K. The two ordered phase transitions have been found in $TmGa_3$, however their transition temperatures are very closed. The one occurs at a Néel temperature of $T_N = 4.26$ K, and the other occurs at a quadrupole antiferromagnetic ordered temperature of $T_Q = 4.29$ K. Below T_N, the magnetism of $TmGa_3$ shows multiaxial anisotropy with a saturation moment of 2.3 μ_B at a temperature of 2 K. As for $ErGa_3$, it shows a modulated antiferromagnetic structure at low temperature, its Néel temperature is 2.8 K, which is close to the second phase transition temperature. It indicates that these transitions occur at very low temperature, thus, it is necessary to improve the magnetic characteristics of RGa_3 for developing novel room temperature diluted magnetic alloy $RGa_{3-x}T_x$ (T = Mn, Co) by doping minor magnetic impurities such as Mn or Co and searching for its potential application as magnetoelectric functional material.

As is well known, the 3d transition metal Mn plays an important role in magnetic materials due to its significant contribution to the magnetic anisotropy by coupling with 4f electrons of the rare-earth.[19–21] Doping Mn into $GdIn_3$ leads to a strong correlation between electric transport and magnetic state, and the electric transitions are associated with the magnetic transitions due to the Stoner spin fluctuation with the increase of temperature. In this study, Mn-diluted $ErGa_3$ magnetic alloy is designed for providing the possibility of the exchange interaction between 3d electrons of Mn and 4f electrons of Er and for expecting to modulate the magnetic characteristics of Mn diluted in $ErGa_3$ magnetic alloy.

2. Experimental details

The samples were prepared according to the normal structural formula of $ErGa_{3-x}Mn_x$ ($x = 0$–0.3) and the purities of raw metals were higher than 99.9 wt%. Owing to the evaporation loss of Er and Mn in the melting process, their weights are appropriately compensated for by supplying extra contents for

*Project supported by the National Natural Science Foundation of China (Grant No. 11274110).

†Corresponding author. E-mail: yqguo@ncepu.edu.cn

© 2019 Chinese Physical Society and IOP Publishing Ltd

Er: 1%∼ 2% and Mn: 8%∼ 10%. The samples were melted in the non-consumable vacuum arc furnace under atmosphere of high pure argon gas. Each sample was re-melted four times to ensure the homogeneity, and followed by being annealed at 800 °C for 168 h in the evacuated quartz tube in order to eliminate the residual stress, and finally by quenching in water.

2.1. Crystal structure analysis

The crystal structures of samples were determined by x-ray diffraction (XRD) with Cu–$K_{\alpha 1}$ radiation, and then the diffraction data were selected for determining crystal structure with TREOR and Rietveld powder diffraction profile fitting technique.

2.2. Magnetic property analysis

The field dependence of magnetization curves (M–H) were measured with a vibrating sample magnetometer (VSM) under the applied fields ranging from −20 kOe (1 Oe = 79.5775 A·m^{-1}) to 20 kOe at room temperature.

3. Results and discussion

3.1. Crystal structure

As shown in Fig. 1(a), the XRD patterns show that $ErGa_{3-x}Mn_x$ alloys are of single phase for $x = 0$ and 0.1, the satellite peaks of the second phase are present in the other two samples with $x = 0.2$ and 0.3. These peaks can be indexed by a hexagonal structure with a group of $P6/mmm$. The planar indices show that the lattice parameters and the crystal cell volumes of cubic phase increase monotonically with the increase of Mn content as listed in Table 1. It is due to the size effect at Ga site. The atomic radii are 1.73 Å for rare earth Er, 1.30 Å for Ga, and 1.40 Å for Mn, respectively. Since the atomic radius of Mn is larger than that of Ga, the substitution of Mn for Ga causes both the lattice parameters and the unit cell volumes to increase. Figure 1(b) is the enlarged plot of Fig. 1(a) around the strongest diffraction peak (111) of cubic phase, and it is very clear that the (111) peak shifts toward the low angle with the increase of Mn content, which causes the planar distance to increase and induces the lattice parameters to augment.

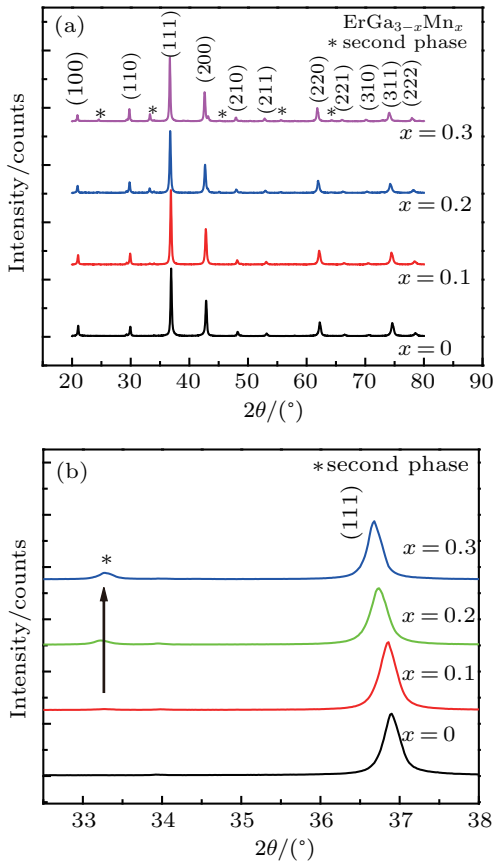


Fig. 1. XRD patterns of (a) $ErGa_{3-x}Mn_x$ alloys and (b) enlarged patterns in 2θ ranging from 32° to 38°.

Table 1. Lattice parameters of cubic $ErGa_{3-x}Mn_x$ alloys.

Lattice parameter	a/Å	V/Å^3
$x = 0$	4.2155	74.911(3)
$x = 0.1$	4.2218	75.247(6)
$x = 0.2$	4.2299	75.681(6)
$x = 0.3$	4.2416	76.311(3)

3.2. Rietveld structure refinement

The crystal structure of $ErGa_{3-x}Mn_x$ was refined by using the Rietveld refinement method. Figures 2(a)–2(d) show the refined XRD patterns of $ErGa_{3-x}Mn_x$ alloys, where the measured and calculated XRD patterns are marked with the symbol of "+" and solid lines, respectively. The lowest trace indicates the differences between the two patterns. Based on the structural refinement, $ErGa_{3-x}Mn_x$ crystallizes into a cubic $AuCu_3$-type structure with a space group of $Pm\bar{3}m$ in an Mn content range of $x < 0.2$.The atomic occupations correspond to 1a (0, 0, 0) site for Er atoms, and 3c (0, 1/2, 1/2) site for (Ga, Mn) atoms. The lattice parameter $a = 4.2155$ Å–4.2416 Å. The crystallographic data are supplied in Tables 2 and 3. In the regime of $x \geq 0.2$, the disordered hexagonal phase coexists with the cubic phase and its structural formula is $Er_{0.8}Ga^{I}_{2}(Ga^{II}, Mn)_{0.4}$, and it can be considered as the derivation of cubic ErGa 1:3 phase; if the number of Er atoms is normalized, the structural formula is written as $ErGa_{2.5}(Ga, Mn)_{0.5}$, *i.e.*, $Er(Ga, Er_{0.8}Ga^{I}_{2}(Ga^{II}, Mn)_{0.4}Mn)$ 1:3. Thus, the disordered $Er(Ga, Mn)_3$ alloy is of hexagonal phase. There are three kinds of nonequivalent crystal positions in this disordered hexagonal unit cell, which are occupied by Er at 1a site, Ga^{I} at 2d site, and (Ga^{II}, Mn) at 2e, respectively. The phase formation is induced by substituting the (Ga^{II}, Mn)–(Ga^{II}, Mn) pair at 2e crystal position for rare earth Er at 1a site. According to the refined results, the corrected formulae of $ErGa_{3-x}Mn_x$ cubic phase are $ErGa_{2.91}Mn_{0.09}$ for $x = 0.1$, $ErGa_{2.79}Mn_{0.21}$ for $x = 0.2$, and $ErGa_{2.71}Mn_{0.29}$ for $x = 0.3$, respectively. The formulae of disorderedly hexagonal phase are $Er_{0.8}Ga_2(Ga_{0.88}Mn_{0.12})_{0.4}$ for $x = 0.2$ and $Er_{0.8}Ga_2(Ga_{0.10}Mn_{0.90})_{0.4}$ for $x = 0.3$. Since the

Mn content increases in the two phases, their lattice parameters and unit cell volumes rise up correspondingly. The content of muti-phase can be determined from the following formula according to the structural refinement parameters:[22]

$$\omega_i = \frac{S_i Z_i M_i V_i}{\sum_i S_i Z_i M_i V_i}, \quad (1)$$

where ω_i is the weight percentage of the i-th phase, S_i, Z_i, M_i, and V_i represent the scale factor, the number of formula units per unit cell, molecular weight, and cell volume in the i-th phase. The calculated weight percentages of $ErGa_{2.79}Mn_{0.21}$, $Er_{0.8}Ga_2(Ga_{0.88}Mn_{0.12})_{0.4}$, $ErGa_{2.71}Mn_{0.29}$, and $Er_{0.8}Ga_2(Ga_{0.10}Mn_{0.90})_{0.4}$ are 92.58%, 7.42%, 91.55%, and 8.45%, respectively.

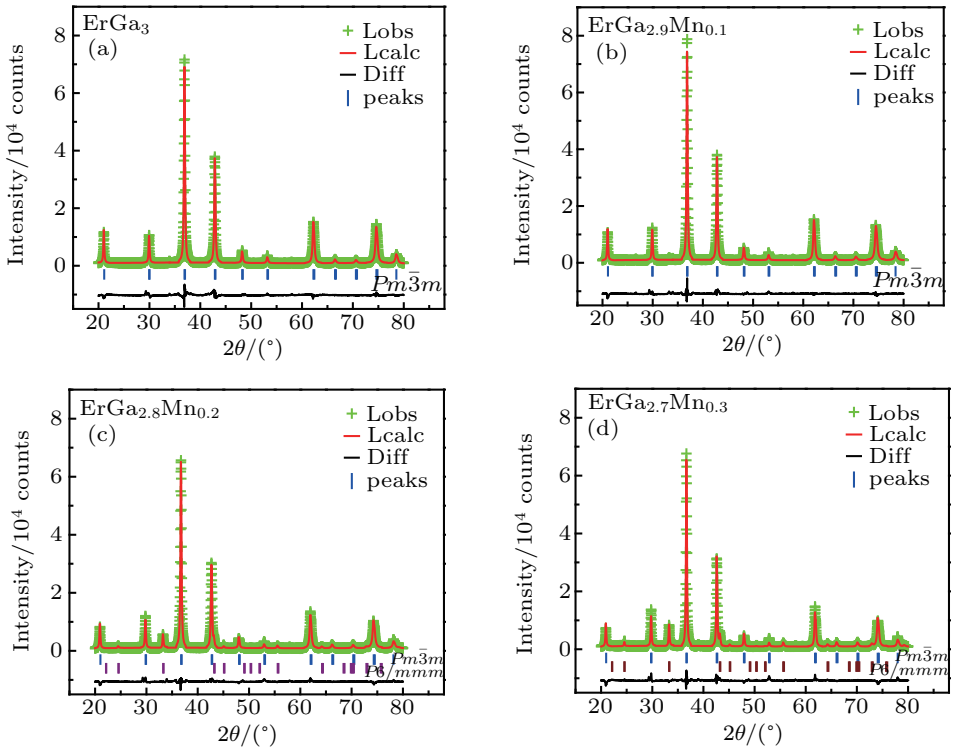


Fig. 2. Observed and calculated XRD patterns of $ErGa_{3-x}Mn_x$ for (a) $x = 0$, (b) $x = 0.1$, (c) $x = 0.2$, and (d) $x = 0.3$.

Table 2. Rietveld refinement structural parameters of $ErGa_{3-x}Mn_x$.

Sample		$ErGa_3$	$ErGa_{2.9}Mn_{0.1}$	$ErGa_{2.8}Mn_{0.2}$	$ErGa_{2.7}Mn_{0.3}$
Space group		$Pm\bar{3}m$	$Pm\bar{3}m$	$Pm\bar{3}m$	$Pm\bar{3}m$
Z		1	1	1	1
a/Å		4.2155	4.2218	4.2299	4.2416
Er 1a	x	0	0	0	0
Number	y	0	0	0	0
	z	0	0	0	0
	N	1	1	1	1
Ga 3c	x	0	0	0	0
Number	y	1/2	1/2	1/2	1/2
	z	1/2	1/2	1/2	1/2
	N	3	2.91	2.79	2.71
Mn 3c	x	–	0	0	0
Number	y	–	1/2	1/2	1/2
	z	–	1/2	1/2	1/2
	N	–	0.09	0.21	0.29
R_p/%		7.086	5.656	5.758	6.908
R_{wp}/%		9.736	8.275	8.181	9.400

Table 3. Rietveld refinement structural parameters of $Er_{0.8}Ga_2^I(Ga^{II}, Mn)_{0.4}$.

Sample		$ErGa_{2.8}Mn_{0.2}$	$ErGa_{2.7}Mn_{0.3}$
Space group		$P6/mmm$	$P6/mmm$
Z		2	2
a/Å		4.1860	4.1856
c/Å		4.0156	4.0145
Er 1a	x	0	0
Number	y	0	0
	z	0	0
	N	0.80	0.80
Ga^I 2d	x	1/3	1/3
Number	y	2/3	2/3
	z	1/2	1/2
	N	2	2
Ga^{II} 2e	x	0	0
Number	y	0	0
	z	0.16011	0.32013
	N	0.35	0.04
Mn 2e	x	0	0
Number	y	0	0
	z	0.16011	0.32013
	N	0.05	0.36
R_p/%		5.758	6.908
R_{wp}/%		8.181	9.400

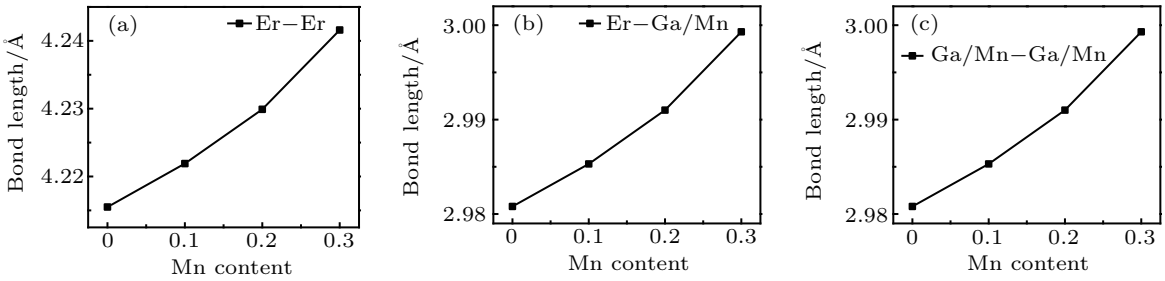


Fig. 3. Mn content-dependent bond lengths of $ErGa_{3-x}Mn_x$ compounds for (a) Er–Er, (b) Er–(Ga, Mn), and (c) (Ga, Mn)–(Ga, Mn).

The bond lengths in $ErGa_{3-x}Mn_x$ intermetallic compounds are calculated according to the refined atomic coordinates and the results are shown in Figs. 3(a)–3(c). Since the radius of Mn atom (1.40 Å) is larger than that of Ga atom (1.30 Å), doping Mn into $ErGa_3$ causes both the lattice parameters and the unit cell volume to increase, which induces significantly the lattice to distort through prolonging the Er–Er, Ga–Ga, and Er–Ga bond lengths as listed in Table 4. The driving force for forming the disordered $Er_{0.8}Ga_2(Ga, Mn)_{0.4}$ phase might be due to the lattice distortion. The substitution of Mn for Ga reduces the effective atomic radius ratio between Er and (Ga, Mn) and forms the structural skeleton of $Er_{0.8}Ga_2(Ga, Mn)_{0.4}$. The projections of unit cells for the two structures reveal that the phase transformation from the cubic $ErGa_3$ to hexagonal $Er_{0.8}Ga_2(Ga, Mn)_{0.4}$ originates from the rotation of $M6$ (M = Ga, Mn) hexagonal ring.[23] Comparing with the projection along the [111] direction in $ErGa_3$, the $M6$ hexagonal ring rotates an angle of 30° in $Er_{0.8}Ga_2(Ga, Mn)_{0.4}$ as shown in Fig. 4.

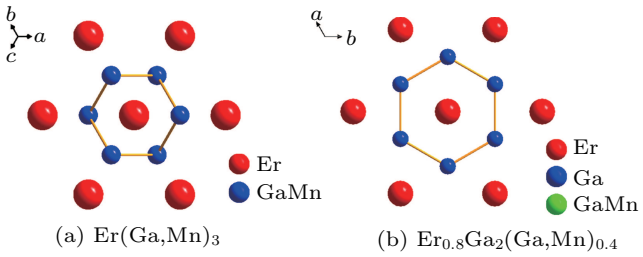


Fig. 4. Projections of cubic $ErGa_3$ along [111] direction and hexagonal $ErGa_2(Ga, Mn)_{0.4}$ along [001] direction for (a) cubic structure and (b) hexagonal structure.

Table 4. Bond lengths of cubic $ErGa_{3-x}Mn_x$.

		$ErGa_3$	$ErGa_{2.9}Mn_{0.1}$	$ErGa_{2.8}Mn_{0.2}$	$ErGa_{2.7}Mn_{0.3}$
Bond length/Å	Er–Ga/Mn	2.9808	2.9853	2.9910	2.9993
	Er–Er	4.2155	4.2218	4.2299	4.2416
	Mn/Ga–Mn/Ga	2.9808	2.9853	2.9910	2.9993

3.3. Magnetic properties

Figure 5 shows the observed and fitted magnetization curves by using vibrating sample magnetometer (VSM) at room temperature, where the symbols of circle and solid lines are corresponding to the observed and fitted magnetization, respectively. The $ErGa_{3-x}Mn_x$ is paramagnetic based on its linear magnetizing characterization through fitting the following equation:

$$M = \chi H, \tag{2}$$

where M, χ, and H are corresponding to the magnetization, paramagnetic susceptibility, and external field. The magnetization rises up with Mn content increasing and reaches the saturation level at Mn content of $x = 0.1$. The fitting parameters are listed in Table 5. The Mn content-dependent a and V, susceptibility χ are shown in Figs. 6(a) and 6(b), respectively. The paramagnetic susceptibility variation tendency can be due to Mn ion and Er ion increasingly contributing to effective moments, however, the susceptibility comes down in the two-phase regime of $x > 0.1$, which can be due to the presence of second phase $Er_{0.8}Ga_2(Ga, Mn)_{0.4}$, and the phase content of the second phase increasing with Mn content. According to Mn content dependence of susceptibility shown in Fig. 6(b) and Mn–Mn bond lengths listed in Table 4, the lattice distortion relative to the paramagnetic susceptibility, the prolongations of Er–Er and Mn–Mn bond lengths cause the susceptibility to decrease in the two-phase region.

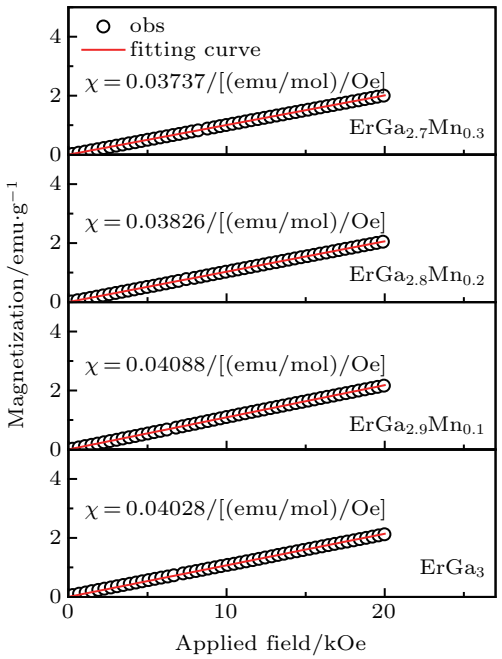


Fig. 5. Observed and fitted magnetization curves of $ErGa_{3-x}Mn_x$ alloys at room temperature.

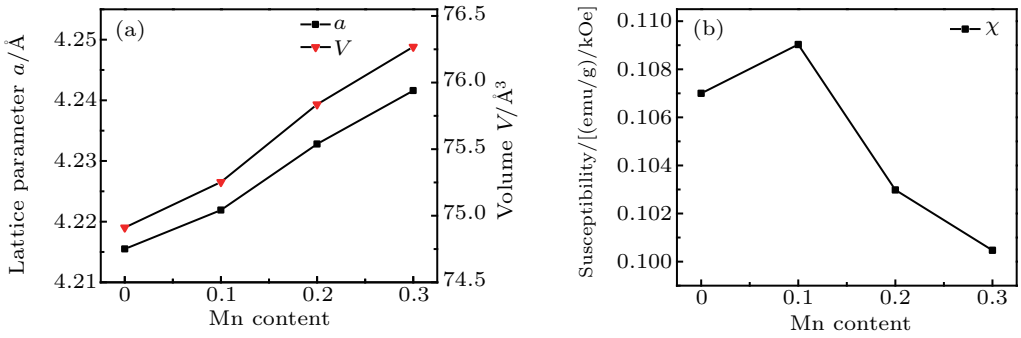


Fig. 6. Curves of Mn content-dependent fitted parameters of $ErGa_{3-x}Mn_x$ for (a) lattice parameter a and volume V, and (b) susceptibility χ.

Table 5. Fitted parameters of $ErGa_{3-x}Mn_x$.

Samples		$ErGa_3$	$ErGa_{2.9}Mn_{0.1}$	$ErGa_{2.8}Mn_{0.2}$	$ErGa_{2.7}Mn_{0.3}$
Reduced chi-sqr		3.45072×10^{-4}	2.9072×10^{-5}	3.01632×10^{-6}	3.52715×10^{-6}
Adj. *R*-square		0.9991	0.99993	0.99999	0.99999
Value/(emu/g/kOe)	χ	0.107	0.10903	0.10298	0.10047
Standard error	χ	1.1153×10^{-4}	3.2519×10^{-5}	1.05198×10^{-5}	1.13459×10^{-5}

4. Conclusions

The Mn doped $ErGa_{3-x}Mn_x$ alloys crystallize into cubic structure with a space group of $Pm\bar{3}m$ in a range of $x = 0$–0.1. The phase separation from cubic phase to disordered hexagonal phase occurs in each of the samples with $x = 0.2$ and 0.3. Rietveld structural refinements show that the structural formula of disordered hexagonal phase is $Er_{0.8}Ga^{I}_{2}(Ga^{II}, Mn)_{0.4}$ with the space group of $P6/mmm$ and $Z = 2$. There are three kinds of nonequivalent crystal positions in unit cell, which are occupied by Er at 1*a* site, Ga^{I} at 2*d* site, and (Ga^{II}, Mn) at 2*e*, respectively. The phase formation of disordered hexagonal phase is induced by substituting the (Ga^{II}, Mn)–(Ga^{II}, Mn) pair at 2*e* crystal position for the rare earth Er at 1*a* site. The lattice parameters tend to increase with Mn content increasing due to the size effect at Ga (1.30 Å) site by substituting Mn (1.40 Å) for Ga.

The $ErGa_{3-x}Mn_x$ alloys show paramagnetic characteristics at room temperature. With the increase of Mn content in a range of $x = 0$–0.1, the magnetic susceptibility χ increases due to the Mn ion and Er ion increasingly contributing to effective moment. However, the magnetic susceptibility χ decreases with Mn content increasing, which is due to the phase separation from the cubic $Er(Ga, Mn)_3$ to $Er_{0.8}Ga_2(Ga, Mn)_{0.4}$. The lattice distortion is the phase transition driving force and causes the Er–Er and Mn–Mn bond lengths to be prolonged, which induces the susceptibility to decrease.

References

[1] Buschow K H J 1979 *Rep. Prog. Phys.* **42** 1373
[2] Lawrence J 1979 *Phys. Rev. B* **20** 3770
[3] Bross H 2011 *Adv. Cond. Matter Phys.* **2011** 867074
[4] Belyavina N, Nakonechna O, Babich M and Markiv V 2015 *J. Alloys Compd.* **643** 137
[5] Solyga A, Czopnik A, Pluznikov V, Ulner J, Durczewski K and Kletowski Z 2006 *European Conference on Physics of Magnetism (PM 05), June 24–27, 2005, Poznan, Poland*, p. 159
[6] Pluzhnikov V B, Grechnev G E, Czopnik A and Eriksson O 2005 *Low. Temp. Phys.* **31** 313
[7] Slater B R, Bie H Y, Stoyko S S, Bauer E D, Thompson J D and Mar A 2012 *J. Solid. State. Chem.* **196** 409
[8] Pluzhnikov V B, Czopnik A and Svechkarev I V 1995 *Physica B* **212** 375
[9] Kletowski Z 1992 *Solid. State. Commun.* **83** 241
[10] Shafiq M, Ahmad I and Asadabadi S J 2014 *J. Appl. Phys.* **116** 103905
[11] Chen S L, Guo Y Q and He Q 2015 *J. Appl. Phys.* **117** 123910
[12] Kletowski Z, Fabrowski R, Slawiński P and Henkie Z 1997 *J. Magn. Magn. Mater.* **166** 361
[13] Kletowski Z 2000 *Supermaterials* (Netherlands: Springer) pp. 163–172
[14] Kletowski Z, Czonpnik A, Tal A and Boer F D 2000 *Physica B* **281–282** 163
[15] Cirafici S and Franceschi E 1981 *J. Less. Comm. Met.* **77** 269
[16] Murtaza G, Gupta S, Seddik T, Khenata R, Alahmed Z, Ahmed R, Khachai H, Jha P and Omran S 2014 *J. Alloys Compd.* **597** 36
[17] Morin P, Giraud M, Regnault P L, Roudaut E and Czopnik A 1987 *J. Magn. Magn. Mater.* **66** 345
[18] Fulfer B W, McAlpin J D, Engelkemier J, McCandless G T, Prestigiacomo J, Stadler S, Fredrickson D C and Chan J Y 2014 *Chem. Mater.* **26** 1170
[19] Negri D, Kaczorowsiki, Grytsiv, Alleno and Giovannini 2004 *J. Alloys Compd.* **365** 58
[20] Singh S, Dhar S, Manfrinetti P and Palenzona A 2002 *J. Magn. Magn. Mater.* **250** 190
[21] Dhar S, Manfrinetti P and Palenzona A 2002 *Solid. State. Commun.* **124** 379
[22] Hill R J and Howard C J 1987 *J. Appl. Crystallogr.* **20** 467
[23] He Q and Guo Y Q 2016 *Appl. Phys. A* **122** 1